JAERI-M
83-061

CALCULATION OF ABSOLUTE FISSION-RATE DISTRIBUTIONS MEASURED IN GRAPHITE-REFLECTED LITHIUM OXIDE BLANKET ASSEMBLY

April 1983

Yasushi SEKI, Hiromitsu KAWASAKI*, Hiroshi MAEKAWA,
Yukio OYAMA, Yujiro IKEDA and Tomoo NAKAMURA

日本原子力研究所
Japan Atomic Energy Research Institute

JAERI-Mレポートは、日本原子力研究所が不定期に公刊している研究報告書です。
入手の問合わせは、日本原子力研究所技術情報部情報資料課（〒319-11茨城県那珂郡東海村）あて、お申しこしください。なお、このほかに財団法人原子力弘済会資料センター（〒319-11茨城県那珂郡東海村日本原子力研究所内）で複写による実費頒布をおこなっております。

JAERI-M reports are issued irregularly.
Inquiries about availability of the reports should be addressed to Information Section, Division of Technical Information, Japan Atomic Energy Research Institute, Tokai-mura, Naka-gun, Ibaraki-ken 319-11, Japan.

編集兼発行　日本原子力研究所
印　　刷　㈱高野高速印刷

Calculation of Absolute Fission-Rate Distributions Measured in Graphite Reflected Lithium Oxide Blanket Assembly

Yasushi SEKI, Hiromitsu KAWASAKI*
Hiroshi MAEKAWA, Yukio OYAMA
Yujiro IKEDA and Tomoo NAKAMURA

Division of Reactor Engineering,
Tokai Research Establishment, JAERI

(Received March 14, 1983)

The fission-rate distributions of ^{232}Th, ^{238}U, ^{237}Np and ^{235}U have been measured in a pseudo-spherical graphite reflected lithium oxide (Li_2O-C) assembly in 1978. The 14 MeV neutrons were generated at the center of the assembly by the D-T reaction with a 300 kV Cockcroft-Walton type accelerator called PNS-A. The fission rates are calculated using the newly evaluated nuclide densities and current nuclear data.

As a result, the calculated and measured fission rates mostly agreed within the estimated experimental error. The agreement is particularly good in the Li_2O region indicating the validity of the calculated neutron spectra in the region. The calculation underestimates the ^{232}Th fission rate in the graphite region. The calculation overestimates the ^{235}U fission rate by about 15% in the graphite region near the Li_2O region.

KEYWORDS: D-T Neutron, Lithium Oxide, Graphite Reflector, Blanket, Measurement, Calculation, Nuclear Data, Fusion Reactor, PNS-A, Fission Chamber

---

* Century Research Center Corporation Ltd.

黒鉛反射体付酸化リチウムブランケット体系における核分裂率分布絶対値測定の計算

日本原子力研究所東海研究所原子炉工学部
関　　泰・川崎　弘光*・前川　　洋・大山　幸夫
池田裕二郎・中村　知夫

（１９８３年３月１４日受理）

１９７８年に黒鉛反射体付酸化リチウムの擬似球形体係において^{232}Th，^{238}U，^{237}Npと^{235}Uの核分裂率分布が測定された。この体系の中心において１４MeV中性子をD－T反応により３００kVコッククロフト・ウォルトン型加速器PNS－Aを用いて発生させた。核分裂率分布を最近評価し直した原子数密度と最新の核データを用いて計算した。

その結果計算された核分裂率の値は測定値とほぼ実験誤差の範囲内で一致した。両者の一致は酸化リチウム領域で特に良く，この領域における中性子のスペクトルが正しく計算されていることを示している。計算は黒鉛領域における^{232}Thの核分裂率を過小評価している。黒鉛領域の酸化リチウムに近い位置では^{235}Uの核分裂率を計算値は約１５％過大評価している。

＊　センチュリ・リサーチ・センター（株）

目　　次

CONTENTS

1. INTRODUCTION

In order to check the applicability of the nuclear data and calculational methods used in the nuclear design of fusion reactors, a number of integral experiments have been conducted.[1]-[5] Lithium oxide has been proposed[6] in the Japan Atomic Energy Research Institute (JAERI) as a tritium breeding material and its nuclear characteristics has been investigated by an integral experiment.[4]

The fission-rate distributions of ^{232}Th, ^{238}U, ^{237}Np and ^{235}U have been measured in a pseudo-spherical graphite reflected lithium oxide (Li_2O-C) assembly in 1978.[4] The 14 MeV neutrons were generated at the center of the assembly by the D-T reaction with a 300 kV Cockcroft-Walton type accelerator. The measurements are described in Ref.(4) and their results are also compared with those of a preliminary calculations in Ref.(4). However, an error of not including the secondary neutrons from the inelastic reactions of ^{16}O has been discovered, which resulted in the underestimation by the preliminarily calculated fission rates. Moreover, the nuclide densities of the materials used to construct the Li_2O-C assembly were re-evaluated, which resulted in somewhat different values. Especially, the nuclide density value of graphite is found to be smaller by about 5.5% than the value originally used in the preliminary analysis.

Using the corrected cross sections of ^{16}O and newly evaluated nuclide densities, the fission rate distributions in the Li_2O-C assembly are calculated. In the process, recently evaluated nuclear data are used in place of old ones, and the effect of their replacement on the calculated fission rates is evaluated. In addition, the effects of the differences in the source neutron spectra and group cross section sets are shown.

The fission-rate measurements are described briefly in Section 2. The calculational procedures are described in Section 3 in the order of the calculational model, nuclear data and group cross sections and neutron transport calculations. Results and discussions are given in Section 4 and some concluding remarks in Section 5. In the APPENDIX 1, the 135-group neutron and 21-group gamma ray coupled cross section set GICXFNS for 18 nuclides of interest in terms of fusion neutronics calculation is introduced. In the APPENDIX 2, the calculated fission rates using various data and method are compared for the Li_2O-C

assembly represented by the old nuclide density table.

2. FISSION RATE MEASUREMENT

The pseudo-spherical Li_2O-C assembly was formed by stacking Li_2O and graphite blocks. The Li_2O blocks were made from Li_2O powder by cold pressing and were sealed in a 0.1 mm-thick stainless steel box. The blocks were placed in stainless steel drawers which in turn were inserted into stainless steel lattice to form the assembly. Horizontal and vertical cross sections of the Li_2O-C assembly across the center are shown in Figs.1(a) and (b), respectively.

The absolute fission rates of ^{232}Th, ^{238}U, ^{237}Np and ^{235}U were measured by traversing micro fission chambers along the experimental hole shown in Fig.1(b). Thus the spatial distributions in the direction perpendicular to the deuteron beam were measured. Details of the experimental procedure can be found in Ref.(3) and (4). The measured fission rates in the Li_2O-C assembly are summarized in Table 1. The fission rates and their errors were determined as in Ref.(3).

assembly represented by the old nuclide density table.

2. FISSION RATE MEASUREMENT

The pseudo-spherical Li_2O-C assembly was formed by stacking Li_2O and graphite blocks. The Li_2O blocks were made from Li_2O powder by cold pressing and were sealed in a 0.1 mm-thick stainless steel box. The blocks were placed in stainless steel drawers which in turn were inserted into stainless steel lattice to form the assembly. Horizontal and vertical cross sections of the Li_2O-C assembly across the center are shown in Figs.1(a) and (b), respectively.

The absolute fission rates of ^{232}Th, ^{238}U, ^{237}Np and ^{235}U were measured by traversing micro fission chambers along the experimental hole shown in Fig.1(b). Thus the spatial distributions in the direction perpendicular to the deuteron beam were measured. Details of the experimental procedure can be found in Ref.(3) and (4). The measured fission rates in the Li_2O-C assembly are summarized in Table 1. The fission rates and their errors were determined as in Ref.(3).

3. CALCULATIONAL PROCEDURES

3.1 Calculational Model

A spherical model adopted for the calculations of the Li_2O-C assembly is shown in Fig.2. An isotropic D-T neutron source is assumed to be uniformly distributed in the central sphere of 0.5 cm radius. The region marked "void" in Fig.2 consists of stainless-steel lattice and drawers, while only lattice framework is present in the portion designated "lattice" in Fig.2. The outer radii of the void region, the Li_2O, the graphite and the lattice regions are 3.3, 22.4, 46.8 and 71.8 cm, respectively. The homogenized nuclide densities of respective regions are given in Table 2. These density values are the newly evaluated ones and are different from the ones given in Ref.(4).

3.2 Nuclear Data and Group Cross Sections

Neutron group cross sections for the 8 nuclides in Table 2 which constitute the Li_2O-C assembly are processed from the evaluated nuclear data files. For the nuclides other than ^{12}C and ^{7}Li, the nuclear data in ENDF/B-4[7] are used. For ^{12}C, the data in ENDF/B-5 standard cross section library[8] are used. As for ^{7}Li, the nuclear data in ENDF/B-4 is used with the following modification. The $^{7}Li(n,n'\alpha)T$ reaction cross section in the original ENDF/B-4 is replaced by the one recently evaluated by P.G. Young.[9] In order to preserve the total cross section of ^{7}Li, the elastic cross section has also been changed to compensate for the change introduced by the replacement of the $^{7}Li(n,n'\alpha)t$ reaction.

The 135-group neutron cross sections with the energy group structure shown in Table A.2 is processed from the above nuclear data using the NJOY code.[10] The cross sections are made for the infinite dilution and at 300°K. Constant flux weighting is used to derive group cross sections from point wise data. In order to calculate the fission rates, the 135-group fission cross sections of ^{232}Th, ^{238}U, ^{237}Np and ^{235}U are also calculated using NJOY under the same calculational condition. The four fission cross sections are compared in Fig.3.

In addition to the 135-group neutron cross sections, the 100-group cross sections prepared for the preliminary analysis[3] is also used with some modifications to calculate the fission rates.

These 100-group cross sections are also made with the same nuclear data using the NJOY code. The energy group structure of the set is the same as that of the DLC-2 set.[11] The 1/E weighting is used for the derivation of group cross sections. Cross sections for infinite dilution are obtained for all nuclides except ^{238}U and ^{235}U for which the fission reactions corresponding to natural uranium concentrations are obtained.

As for the thermal cross section of ^{235}U fission reaction, the value of 415 barn is used for both 135-group and 100-group calculations. This value is obtained for the graphite region mixture by using the thermal reactor design code system SRAC.[12] The SRAC code system uses the combination of cell calculation based on collision probability method and ANISN calculation.[13]

3.3 Neutron Transport Calculations

Neutron transport in the Li_2O-C assembly is calculated using the one dimensional discrete ordinates transport code ANISN.[13] The calculational model shown in Fig.2 is used. An isotropic D-T neutron source is generated uniformly from the central sphere of 0.5 cm radius. Three types of source neutron spectra depicted in Fig.4 are used to see their effect on the calculated fission rates. Three spectra are, a broad rectangular source corresponding to the first group source for the 100-group calculation, and the D-T neutron spectra at 0° and 90° to the deuteron beam. The broad rectangular source is used to compare the results of the 100 group and 135 group calculations. The spectrum at 90° is used because the fission rates are measured at this direction. The spectrum at 0° is used to see the dependence of the calculated results on the source neutron spectrum. The P_5-S_{64} approximation is used along with fine mesh interval of about 0.5 cm in the Li_2O and graphite regions.

4. RESULTS AND DISCUSSIONS

The measured fission rates of ^{232}Th and ^{235}U are compared in Fig.5 with the calculated ones obtained from the 100-group calculation. The measured values are shown with solid symbols while the calculated ones are represented by curves and blank symbols. The measured fission rates of ^{238}U and ^{237}Np are not shown in Fig.5 because they agreed mostly with the calculated ones within the experimental error. The experimental errors are smaller than the solid symbols so that they are not shown in the figure.

Figure 5 shows good agreement between the measurement and calculation for both ^{232}Th and ^{235}U fission rates in the Li_2O region. In the graphite region, the calculation systematically underestimates ^{232}Th fission rate and overestimate ^{235}U fission rate.

In order to see the difference between the measured and calculated fission rates in a more distinct manner, the C/E values, the ratio of calculated and experimental values are shown as the function of the radius R from the center in Figs.6a to 6d for the fission rates of ^{232}Th, ^{238}U, ^{237}Np and ^{235}U, respectively. The C/E values for the four calculations, are plotted together in each figure to show the difference in the calculated values arising from the calculation conditions. The range of experimental error is shown with hatched area. Each of the four fission rates will be discussed below in detail.

4.1 ^{232}Th Fission Rate

In Fig.6a, the C/E values of ^{232}Th fission rate calculated for the four calculations all show the same trend in spatial distribution. In the Li_2O region, the C/E values are within the experimental error but they decrease with increasing radius in the graphite region. It is interesting to note that the relative values of the C/E values for the four calculations change very little with the radius. Since ^{232}Th fission rates are dominated by source neutrons and ^{232}Th fission cross section increases with neutron energy at the 13 MeV-16 MeV range (see Fig.3), the calculated fission rate is larger for the calculation with harder source neutron spectrum (see Fig.4).

4.2 ^{238}U Fission Rate

Almost all the calculated fission rates of ^{238}U agree with the measured ones within the experimental error as shown in Fig.6b. The relative values of the C/E values of ^{238}U for the four calculations are in the same order as those of ^{232}Th. The increase of ^{238}U fission cross section in the source neutron energy range (see Fig.3) and the large contribution of the source neutrons to the ^{238}U fission rate again explain the correlation between the magnitude of the calculated fission rates and the hardness of source neutron spectra.
However, considering the similarity in the shape of fission cross sections of ^{232}Th and ^{238}U, the large discrepancy between the calculation and measurement appearing only in the former is somewhat difficult to explain. The energy-group-wise fission rates of ^{232}Th and ^{238}U at various locations were investigated. The investigation showed that the small difference in the fission cross sections was not enough to explain the discrepancy and some other explanation is still required. Calculated neutron spectra at R = 16 cm in the Li_2O region, and at R = 27 cm and 37 cm in the graphite region are shown in Fig. 7 for a 135-group neutron calculation.

4.3 ^{237}Np Fission Rates

The calculated and measured fission rates of ^{237}Np are also in good agreement as shown in Fig.6c. The calculated values are slightly lower than the measured fission rate at R = 10.1 cm. The correlation between the relative magnitudes of calculated fission rate and the hardness of the source neutron spectra can also be observed for ^{237}Np but in lesser degree.

4.4 ^{235}U Fission Rates

The C/E values of ^{235}U fission rate are shown in Fig.6d. The calculated ^{235}U fission rates agree fairly well with the measured ones in the Li_2O region but become larger than the measured ones at R = 26.6 cm in the graphite region. The discrepancy is the largest for the 100-group calculation being about 32% at R = 26.6 cm. The C/E for the 100-group calculation decreases gradually with increasing R in the graphite region but it stays out of the range of the experimental error.

The C/E values for the 135-group calculations also decrease with R in the graphite region and in these cases the C/E values mostly enter the range of the experimental error. The correlation between the magnitude of the C/E values of the 135-group calculations and the hardness of the source neutron spectrum is also apparent for ^{235}U fission rates.

The difference in the calculated ^{235}U fission rates in the graphite region obtained by the 100-group calculation and the 135-group calculations arises mostly from the approximations employed in the calculation of the fission rate caused by the neutrons in the lowest energy group. As described in 3.2, the 415 barn for the thermal cross section of ^{235}U fission reaction is used for both 100-group and 135-group calculations to calculate the fission rate for the lowest energy groups.
Whereas, the energy range of the 100-th group for the 100-group calculation is 0.025 - 0.414 eV and that of the 135-th group is 0.010 - 0.129 eV. By using ~200 barn corresponding to the fission cross section at 0.025 - 0.414 eV in place of 415 barn, the calculated ^{235}U fission rate by the 100-group calculation will decrease by about 20% and will come near the 135-group results. Furthermore, the change of the C/E in the graphite region suggests that the neutrons in the lowest energy group become thermalized and better agreement is obtained with increasing R in the graphite region.

Another cause for the difference between the calculated ^{235}U fission rate in the graphite region is the difference in the weighting function used to derive group cross sections. The 1/E spectrum is used to derive the 100-group cross sections while constant weighting is employed to process the 135-group cross sections. The effect of the difference in the weighting function and the choice of the thermal fission cross section on the calculated ^{235}U fission rate are discussed further in APPENDIX 2.

The underestimation of ^{235}U fission rate at R = 21.5 cm in the Li_2O region and the overestimation at R = 26.6 cm in the graphite region suggest the effect of the media boundary. The one-dimensional modelling of Fig.2 assumes an effective boundary at R = 22.42 cm for the actual boundary formed by the Li_2O and the graphite blocks as shown in Fig.1.

5. CONCLUDING REMARKS

The calculated and measured fission rates of ^{232}Th, ^{238}U, ^{237}Np and ^{235}U mostly agreed within the experimental error. The agreement is particularly good in the Li_2O region indicating the validity of the calculated neutron spectra in the region.

Although the calculated fission rates of ^{238}U and ^{237}Np agreed with the measured ones in the graphite region, the calculated ^{232}Th fission rate became lower than the measured and the discrepancy increased with the radius R from the center. Provided both cross section data are accurate, the small difference in the shape of the fission cross sections of ^{238}U and ^{232}Th is not sufficient to explain the difference in the C/E's of ^{232}Th and ^{238}U.

The calculated ^{235}U fission rates obtained by the 135-group calculations are larger than the measured by as much as 17% at R = 26.6 cm. This discrepancy seems to be caused by the limitation in the one-dimensional modelling of the actual boundary between the Li_2O and graphite regions. They agree mostly with the measurement within the experimental error at the other three locations in the graphite region. The large discrepancy of the ^{235}U fission rates in the graphite region obtained by the 100-group calculation is mainly caused by the inadequate treatment of the fission rate calculation for the 100-th group.

A strong correlation exists between the choice of the source neutron spectrum and the magnitude of calculated fission rates of all four nuclides. The harder neutron spectrum is shown to yield larger calculated fission rate.

ACKNOWLEDGMENT

The authors thank the members of Fusion Nuclear Data Working Group of the Japan Nuclear Data Committee for the investigation of C and ^{7}Li neutron cross sections. They also thank Dr. Tomoo Suzuki of JAERI for his instructions in the execution of PALLAS-TS (now renamed as BERMUDA-1DN) calculation described in the APPENDIX 2. Valuable comments by Dr. Shojiro Matsuura are also deeply appreciated.

REFERENCES

(1) Green, L., "Review of Integral Fusion Blanket Neutronic Experiments," Proc. Fourth Topical Meeting on Technonlogy of Controlled Nuclear Fusion," CONF-801011, King of Prussia, Vol.1, 395 (1980)

(2) Yamamuro, N. et al., "Studies on Fision Blanket Neutronics," Bull. Research Lab. Nucl. Reactors, 7, 43 (1982)

(3) Maekawa, H. and Seki Y., J. Nucl. Sci. Technol., 14[2], 97 (1977), ibid., 14[3], 210 (1977), ibid., 14[9], 680 (1977)

(4) Maekawa, H. et al., J. Nucl. Sci. Technol., 16[5], 377 (1979)

(5) Nakamura, T. et al., "Integral Experiments on Lithium Oxide Spherical Assembly with Graphite Reflector and on Duct Streaming," Proc. Third IAEA Technical Committee Meeting and Workshop on Fusion Reactor Design and Technology, Tokyo, Oct.5-16, 1981, to be published

(6) Sako, K. et al., "Conceptual Design of a Gas-Cooled Tokamak Reactor," Nucl. Fusion, Special Suppl., Fusion Reactor Design Problems, 27(1974); JAERI-M 5502 (1973)

(7) Drake, M.K. (eidted), "Data Formats and Procedures for the ENDF Neutron Cross Section Library," BNL-50274 (T-601, TID-4500), ENDF 102, Vol.1 (1970), Revised 1974

(8) Fu, C.Y. and Perey, F.G., "New Evaluation of C for Version V, MAT 1306", Oak Ridge National Laboratory (1979)

(9) Young, P.G., Trans. Am. Nucl. Soc., Vol.39, 272 (1981)

(10) MacFarlane, R.E. et al., "The NJOY Nuclear Data Processing System: User's Manual," LA-7584-M (ENDF-272) (1978)

(11) RSIC Data Library Collection, "100 Group Neutron Cross Section Data Based on ENDF/B, DLC-2," Radiation Shielding Information Center, Oak Ridge National Laboratory (1972)

(12) Tsuchihashi, K. et al., "Benchmark Calculations by the Thermal Reactor Nuclear Design Code System SRAC," JAERI-M 9781 (1981) in Japanese

(13) Engle, W.W. Jr., "A User's Manual for ANISN, A One-Dimensional Discrete Ordinates Transport Code with Anisotropic Scattering," K-1693, Computing Technology Center, Union Carbide Corporation (1967)

(14) Kawasaki, H. and Seki, Y., "APPLE-2: An Improved Version of APPLE Code for Plotting Neutron and Gamma Ray Spectra and Reaction Rate," JAERI-M 82-091 (1982)

(15) Miyasaka, S. et al., "GAMLEG-JR, A Production Code of Multigroup Cross Sections and Energy Deposition Coefficients for Gamma-Rays," JAERI-M 6936 (1977)

(16) Rhoades, W.A. and Mynatt, F.R., "The DOT-III Two Dimensional Discrete Ordinates Transport Code," ORNL-TM-4280 (1973)

(17) Suzuki, T., Ishiguro, Y. and Matsui, Y., "PALLAS-TS: A one-Dimensional Neutron Transport Code for Analyzing Fusion Blanket", JAERI-M 9492 (1981) (in Japanese)

(18) Hasegawa, A., PROF-GROUCH-GII, to be published

(19) Seki, Y. and Iida, H., "Coupled 42-group Neutron and 21-Group Gamma Ray Cross Section Sets for Fusion Reactor Calculations," JAERI-M 8818 (1980)

Table 1 Absolute fission rate in Li_2O-C assembly

R (cm)	Absolute fission rate (fission/atom per 14 MeV source neutron)			
	^{235}U	^{238}U	^{237}Np	^{232}Th
10.1	(4.37±0.22)-27†	(1.00±0.10)-27	(2.97±0.22)-27	(3.13±0.34)-28
15.6	(2.97±0.15)-27	(3.47±0.25)-28	(1.09±0.72)-27	(1.06±0.09)-28
21.1	(3.17±0.16)-27	(1.58±0.10)-28	(5.45±0.36)-28	(4.66±0.40)-29
26.6	(6.78±0.33)-27	(7.92±0.57)-29	(2.98±0.21)-28	(2.59±0.24)-29
32.2	(8.00±0.40)-27	(4.32±0.32)-29	(1.63±0.12)-28	(1.48±0.13)-29
37.7	(6.56±0.31)-27	(2.48±0.19)-29	(9.08±0.70)-29	(8.53±0.79)-30
43.3	(3.98±0.19)-27	(1.27±0.10)-29	(4.86±0.40)-29	(4.96±0.45)-30

† Read as $(4.37\pm0.22)\times10^{-27}$

Table 2 Nuclide densities of each region in Li_2O-C assembly

Nuclide	Nuclide density (10^{24} atoms/cm^3)			
	Void	Li_2O	Graphite	Lattice
^6Li		3.355-3*		
^7Li		4.186-2		
O		2.261-2		
C			6.930-2	
Cr	1.751-3	1.935-3	1.751-3	1.161-3
Mn	8.185-5	9.632-5	8.185-5	5.632-5
Fe	6.349-3	7.030-3	6.349-3	4.159-3
Ni	7.303-4	8.106-4	7.303-4	4.821-4

* Read as 3.355×10^{-3}

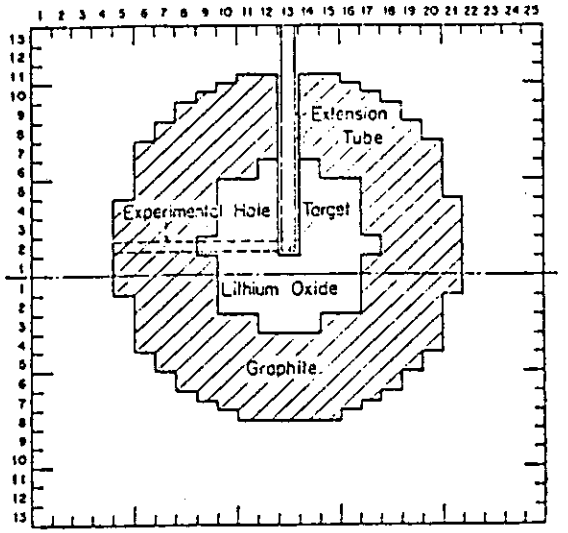

(a) Horizontal section

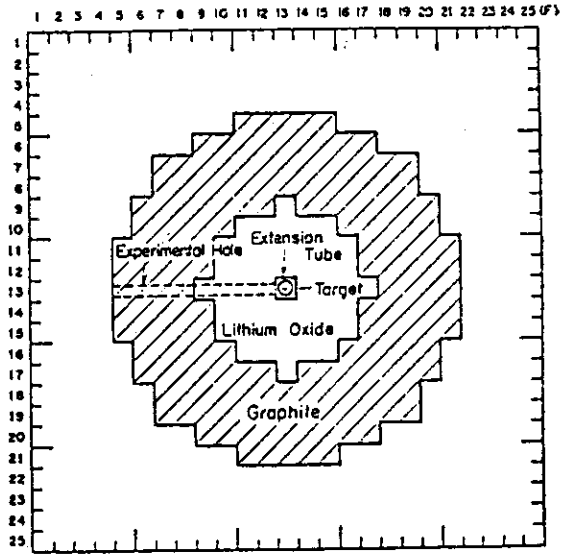

(b) Vertical section

Fig. 1 Horizontal and vertical sections across center of Li_2O-C assembly

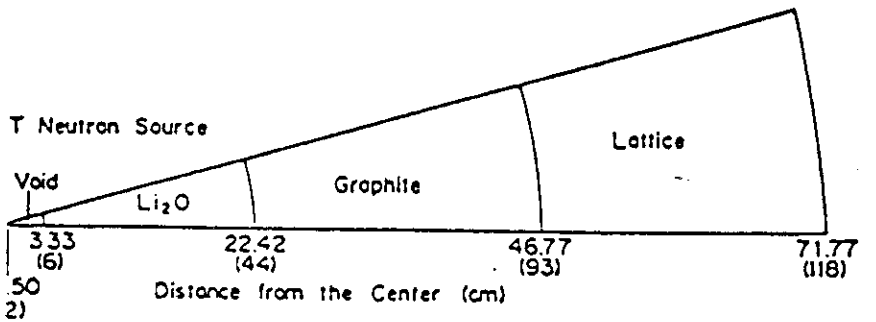

Numbers in parentheses mean the mesh number of boundary in the calculation.

Fig. 2 Calculational model of Li_2O-C assembly

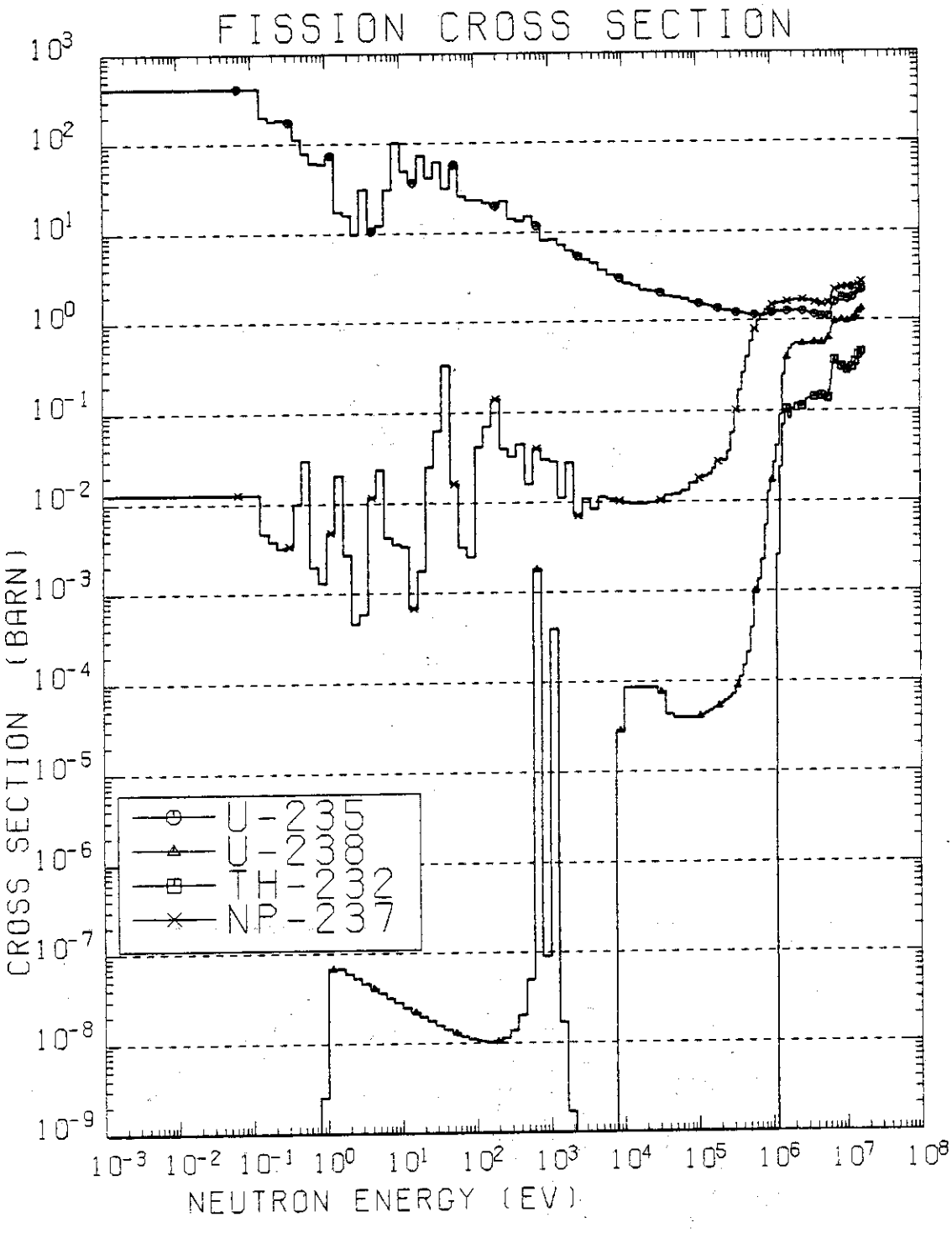

Fig.3 135-Group Fission Cross Sections of ^{232}Th, ^{238}U, ^{237}Np and ^{235}U

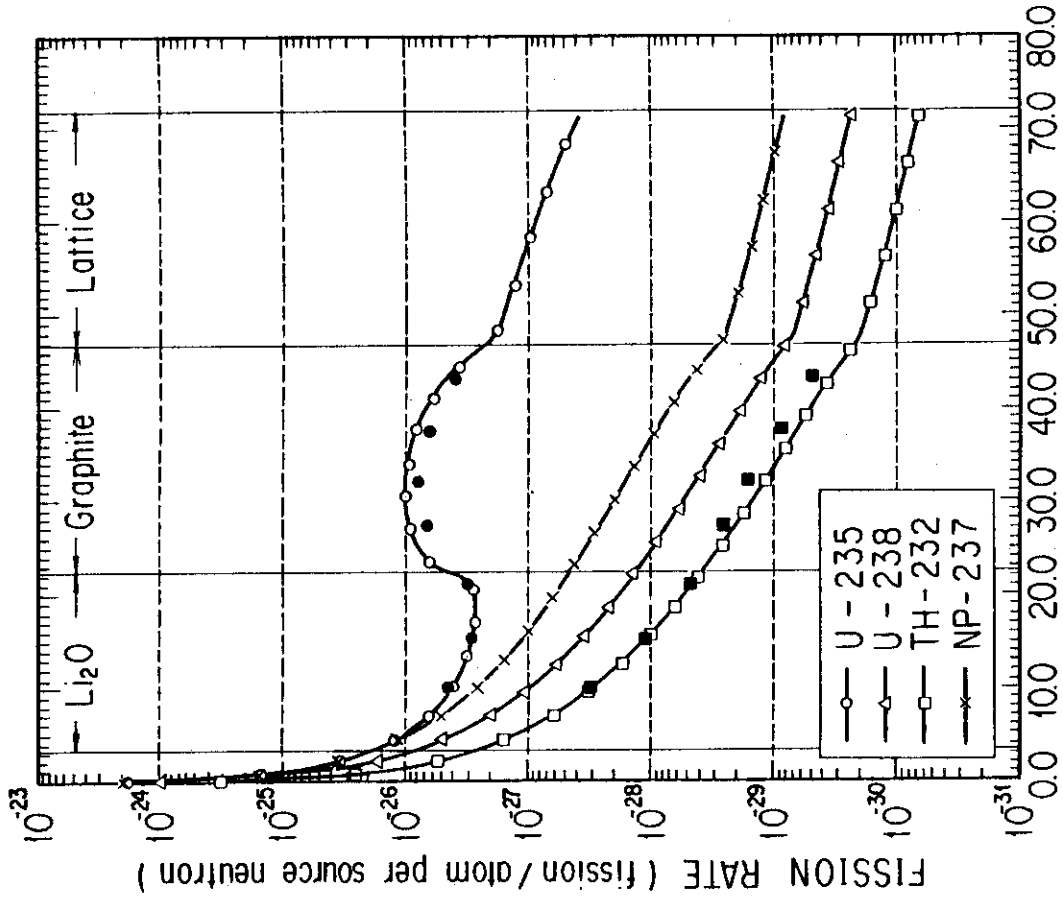

Fig.5 Measured and Calculated Fission Rates in Li_2O-C Assembly

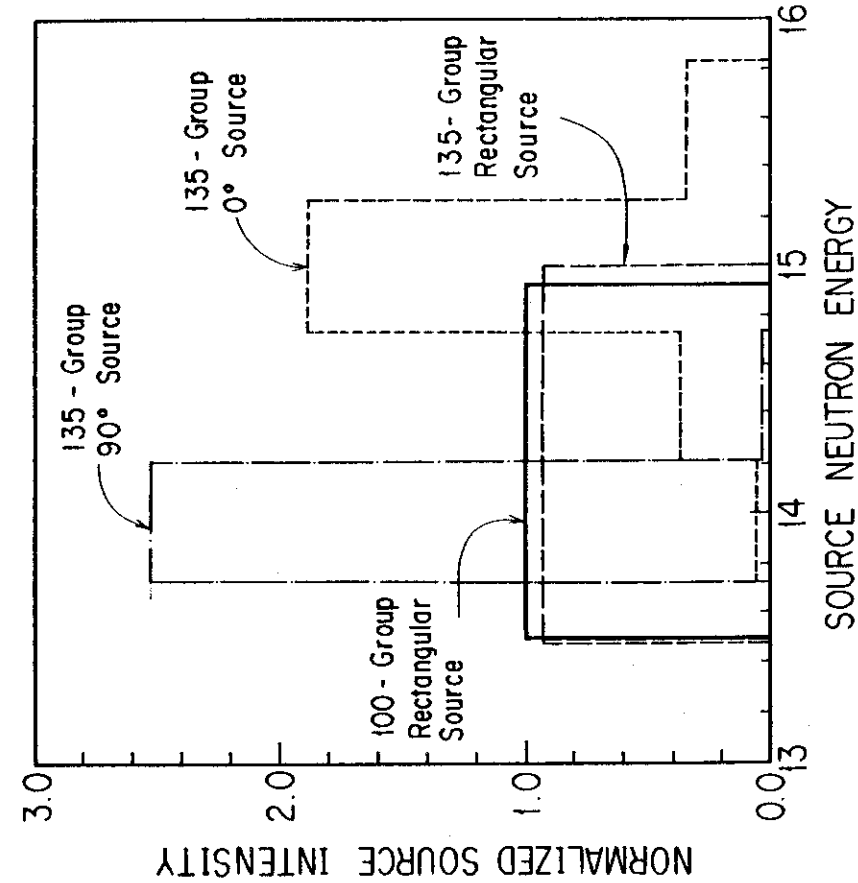

Fig.4 Comparison of Four Source Neutron Spectra Used in the Calculations

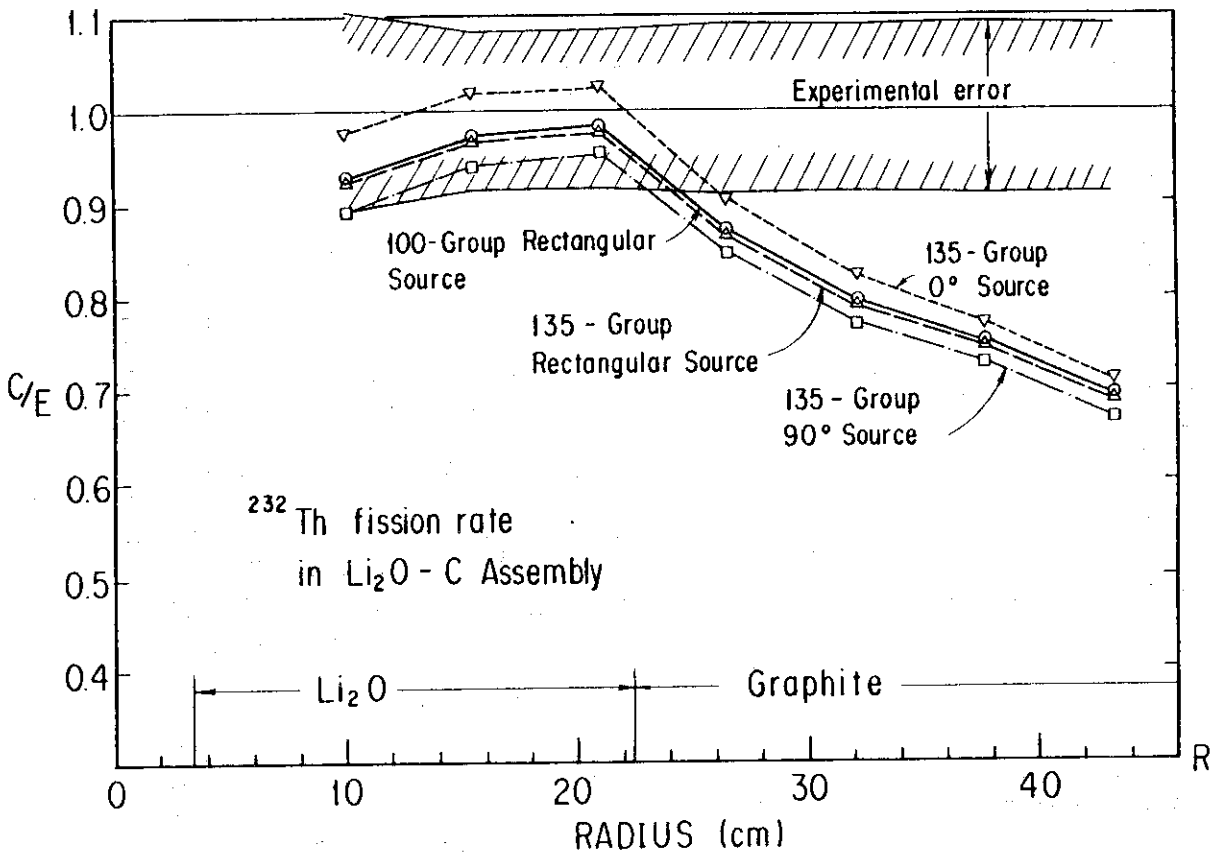

Fig.6a Ratio of Calculated to Experimental C/E Values of ^{232}Th Fission Rate in Li_2O-C Assembly

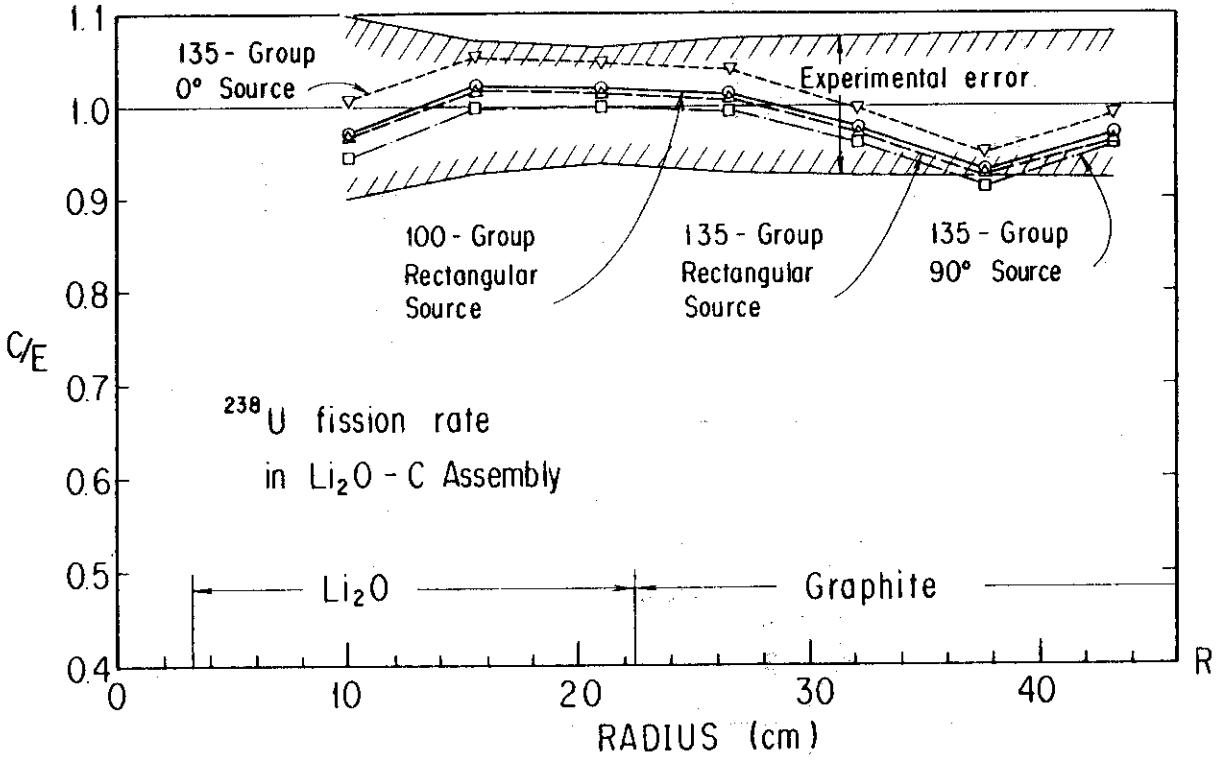

Fig.6b Ratio of Calculated to Experimental C/E Values of ^{238}U Fission Rate in Li_2O-C Assembly

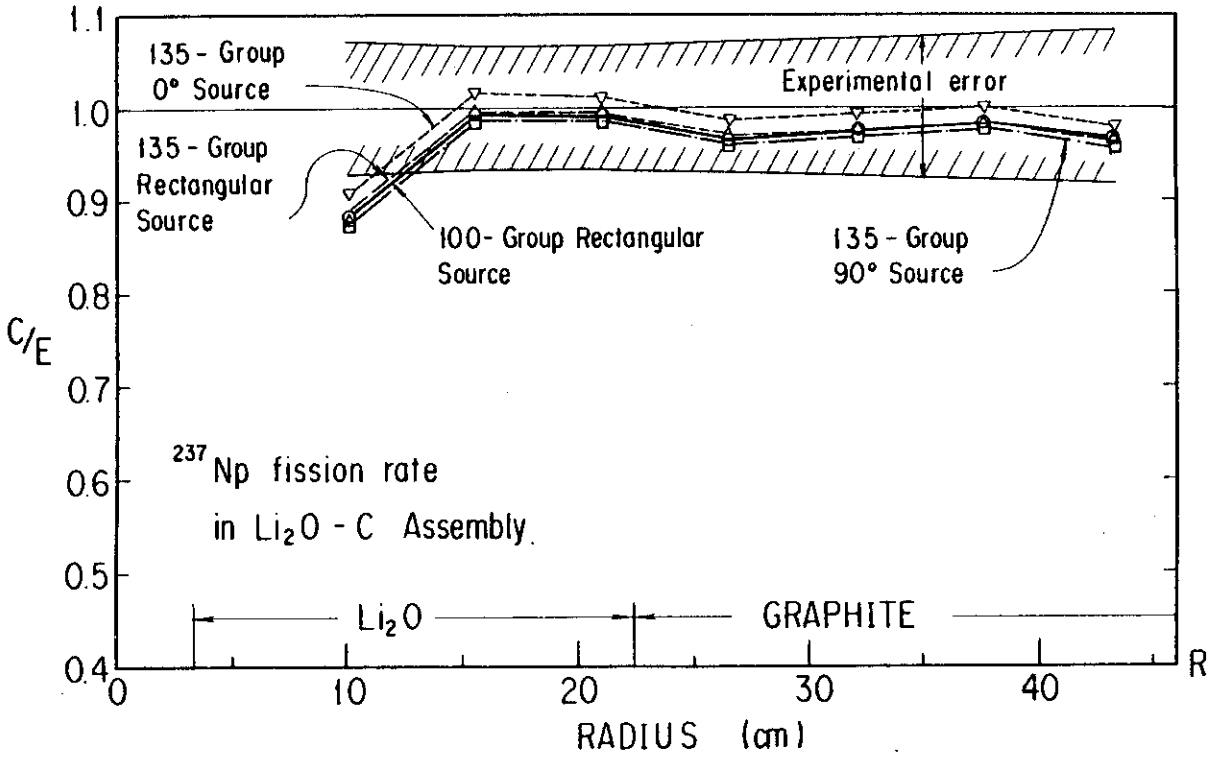

Fig.6c Ratio of Calculated to Experimental C/E Values of ^{237}Np Fission Rate in Li_2O-C Assembly

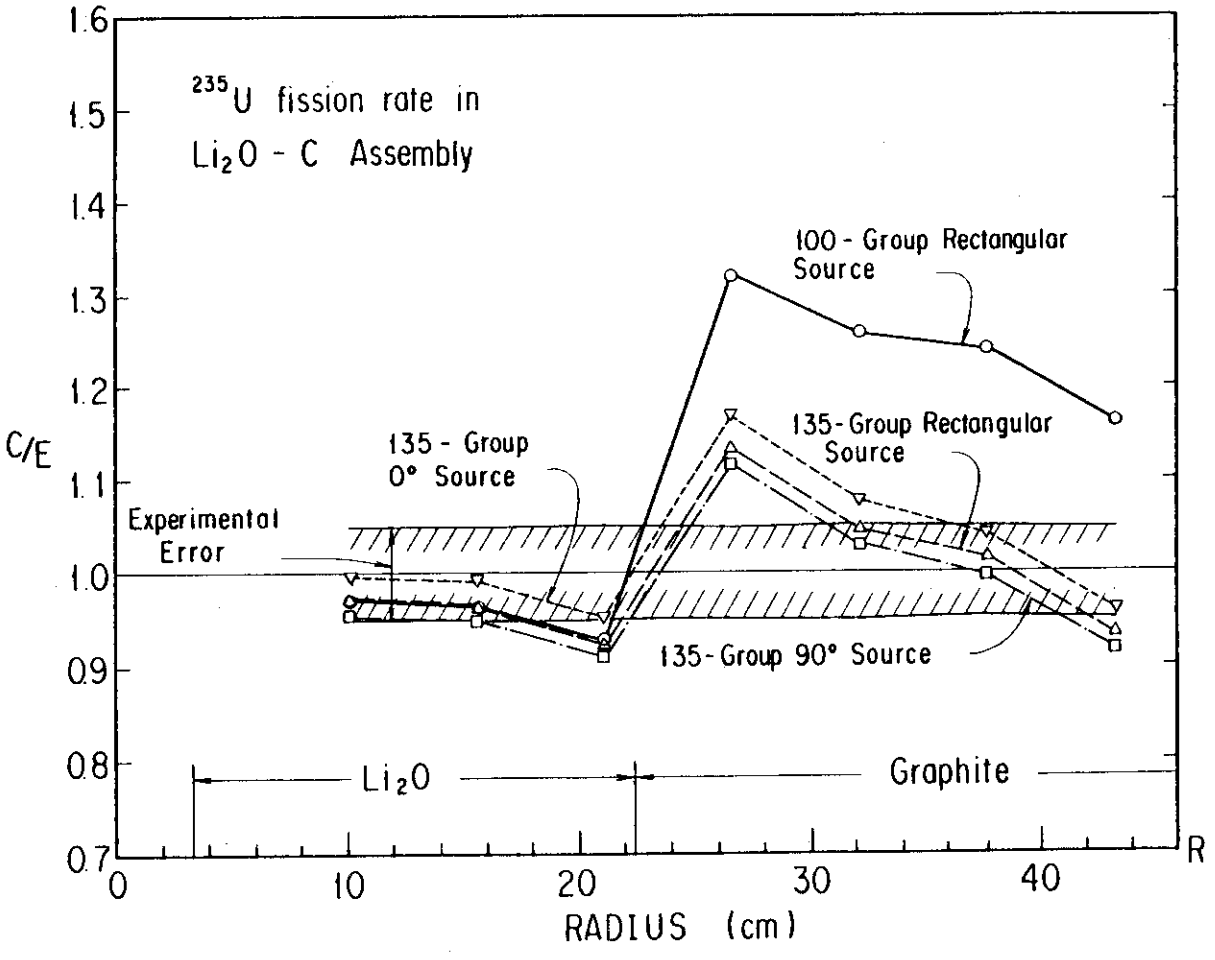

Fig.6d Ratio of Calculated to Experimental C/E Values of ^{235}U Fission Rate in Li_2O-C Assembly

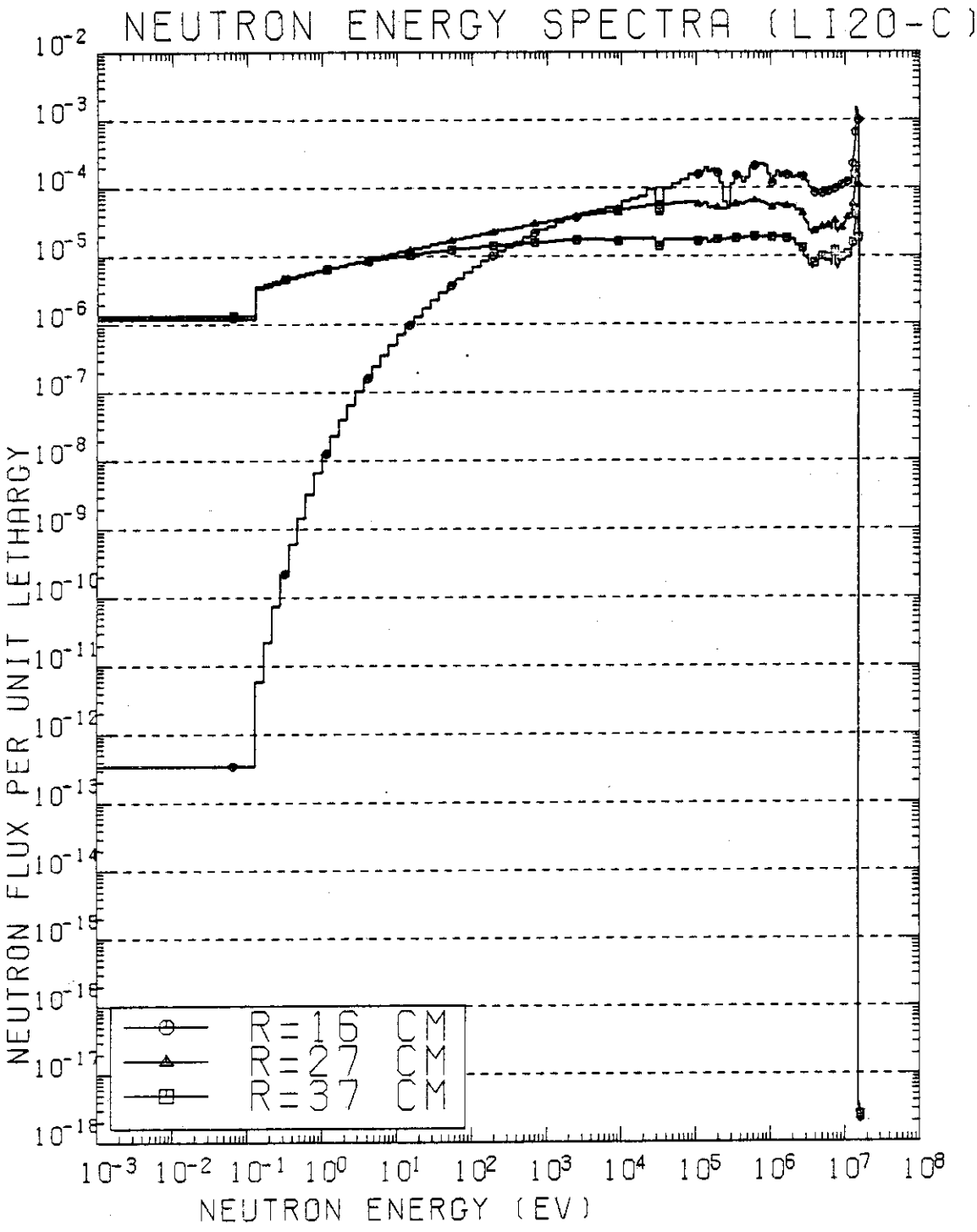

Fig.7 Calculated Neutron Spectra at Three Locations of Li_2O-C Assembly

APPENDIX 1. 135-GROUP NEUTRON, 21-GROUP GAMMA RAY COUPLED CROSS SECTION SET, GICXFNS

A 135-group neutron, 21-group gamma ray coupled cross section set called GICXFNS is developed for the analysis of the neutronics experiments conducted in the Fusion Neutronics Source (FNS) Facility in JAERI.[5] It contains 18 nuclides which will be required in the analysis of the experiments planned using the FNS in the near future. More nuclides will be added as they become necessary. The 18 nuclides are listed in Table A.1 with relevant informations. As shown in the table, all nuclear data are taken from ENDF/B-4[7] except for those for ^{12}C taken from ENDF/B-5[8] and the replacement of the $^{7}Li(n,n'\alpha)t$ cross section according to the recent evaluation.[9] The increment or decrement in the reaction cross section is compensated by the corresponding change in the ^{7}Li elastic reaction to preserve the total cross section.

The energy group structures of the 135-groups for neutron and the 21-groups for gamma ray are shown in Table A.2 and A.3, respectively. The calculational flow for obtaining the coupled cross section set is shown in Fig.A.1. Neutron transport cross sections and gamma ray production cross sections are processed from the above described nuclear data using the NJOY code.[10] The cross sections are made for the infinite dilution and at 300°K. Constant flux weighting is used to derive group cross sections from point wise data. Neutron kerma factors are also obtained using JNOY. Transport cross sections and kerma factors of gamma ray are calculated using the GAMLEG-JR[15] code. The data obtained by NJOY and GAMLEG-JR are combined to form a neutron-gamma coupled cross section set for each nuclide. Up to P_5 Legendre coefficients are included for each nuclide to take account of the anisotropic scattering. Nuclide-wise coupled cross sections for the 18 nuclides are then combined and rearranged to form group wise cross section which can be readable with the one- and two-dimensional discrete ordinates codes ANISN[13] and DOT-3.5[16], respectively. The cross section table of a P_0-component of a nuclide for the i-th group will be as follows;

table position	reaction cross section
1	kerma factor for the i-th group
2	σ_{ai}
3	$\nu\sigma_{fi}$
4	σ_{ti}
5	$\sigma_{i\to i}$
6	$\sigma_{i-1\to i}$
7	----
	----
i + 4	$\sigma_{1\to i}$

Thus the length of the cross section table becomes 135 + 21 + 4 = 160.

Table A.1 List of Nuclides in GICXFNS Set

No.	Nuclide	MAT No.	FILE	MT No. used in ANISN	Reference other than ENDF/B-4[7]
1	^{1}H	1269	404	1 ~ 6	
2	^{6}Li	1271	404	7 ~ 12	
3	^{7}Li	1272	404	13 ~ 18	$^{7}Li(n,n'\alpha)t$[9]
4	C	1306	511	19 ~ 24	ENDF/B-5[8]
5	^{14}N	1275	408	25 ~ 30	
6	^{16}O	1276	408	31 ~ 36	
7	^{23}Na	1156	403	37 ~ 42	
8	Mg	1280	405	43 ~ 48	
9	$^{27}A\ell$	1193	405	49 ~ 54	
10	Si	1194	405	55 ~ 60	
11	K	1150	403	61 ~ 66	
12	Ca	1195	401	67 ~ 72	
13	Cr	1191	406	73 ~ 78	
14	Mn	1197	409	79 ~ 84	
15	Fe	1192	406	85 ~ 90	
16	Ni	1190	406	91 ~ 96	
17	Cu	1295	410	97 ~ 102	
18	Mo	1287	409	103 ~ 108	

Table A.2 135-group neutron energy group structure

Group	Energy limits	Mid-point energy
1	16.399 - 16.110 MeV	16.2545 MeV
2	16.110 - 15.825	15.9675
3	15.825 - 15.545	15.6850
4	15.545 - 15.270	15.4075
5	15.270 - 15.000	15.1350
6	15.000 - 14.735	14.8675
7	14.735 - 14.474	14.6045
8	14.474 - 14.218	14.3460
9	14.218 - 13.967	14.0925
10	13.967 - 13.720	13.8435
11	13.720 - 13.477	13.5985
12	13.477 - 13.239	13.3580
13	13.239 - 13.005	13.1220
14	13.005 - 12.775	12.8900
15	12.775 - 12.549	12.6620
16	12.549 - 12.182	12.3655
17	12.182 - 11.825	12.0035
18	11.825 - 11.479	11.6520
19	11.479 - 11.143	11.3110
20	11.143 - 10.817	10.9800
21	10.817 - 10.500	10.6585
22	10.500 - 10.089	10.2945
23	10.089 - 9.693	9.8910
24	9.693 - 9.314	9.5035
25	9.314 - 8.949	9.1315
26	8.949 - 8.598	8.7735
27	8.598 - 8.261	8.4295
28	8.261 - 7.938	8.0995
29	7.938 - 7.627	7.7825
30	7.627 - 7.327	7.4770
31	7.327 - 7.041	7.1840
32	7.041 - 6.765	6.9030
33	6.765 - 6.500	6.6325
34	6.500 - 6.242	6.3710
35	6.242 - 5.995	6.1185
36	5.995 - 5.757	5.8760
37	5.757 - 5.529	5.6430
38	5.529 - 5.310	5.4195
39	5.310 - 5.099	5.2045
40	5.099 - 4.897	4.9980
41	4.897 - 4.707	4.8000
42	4.703 - 4.516	4.6095
43	4.516 - 4.337	4.4265
44	4.337 - 4.165	4.2510
45	4.165 - 4.000	4.0825

Table A.2 Continued

Group	Energy limits	Mid-point energy
46	4.000 - 3.699 MeV	3.8495 MeV
47	3.699 - 3.419	3.5590
48	3.419 - 3.162	3.2905
49	3.162 - 2.924	3.0430
50	2.924 - 2.704	2.8140
51	2.704 - 2.500	2.6020
52	2.500 - 2.270	2.3850
53	2.270 - 2.061	2.1655
54	2.061 - 1.871	1.9660
55	1.871 - 1.698	1.7845
56	1.698 - 1.542	1.6200
57	1.542 - 1.400	1.4710
58	1.400 - 1.275	1.3375
59	1.275 - 1.162	1.2185
60	1.162 - 1.058	1.1100
61	1.058 - 0.964	1.0110
62	0.964 - 0.878	0.921
63	0.878 - 0.800	0.839
64	0.800 - 0.713	0.7565
65	0.713 - 0.635	0.6740
66	0.635 - 0.566	0.6005
67	0.566 - 0.504	0.5350
68	0.504 - 0.449	0.4765
69	0.449 - 0.400	0.4245
70	0.400 - 0.356	0.3780
71	0.356 - 0.317	0.3365
72	0.317 - 0.283	0.3000
73	0.283 - 0.252	0.2675
74	0.252 - 0.224	0.2380
75	0.224 - 0.200	0.2120
76	0.200 - 0.178	0.1890
77	0.178 - 0.159	0.1685
78	0.159 - 0.141	0.1500
79	0.141 - 0.126	0.1335
80	0.126 - 0.112	0.1190
81	0.112 - 0.100	0.1060
82	0.100 - 0.0774	0.0887
83	77.4 - 59.9 KeV	68.65 KeV
84	59.9 - 46.4	53.15
85	46.4 - 35.9	41.15
86	35.9 - 27.8	31.85
87	27.8 - 21.5	24.65
88	21.5 - 16.7	19.10
89	16.7 - 12.9	14.80
90	12.9 - 10.0	11.45

Table A.2 Continued

Group	Energy limits	Mid-point energy
91	10.0 - 7.74 KeV	8.870 KeV
92	7.74 - 5.99	6.865
93	5.99 - 4.64	5.315
94	4.64 - 3.59	4.115
95	3.59 - 2.78	3.185
96	2.78 - 2.15	2.465
97	2.15 - 1.67	1.910
98	1.67 - 1.29	1.480
99	1.29 - 1.00	1.145
100	1.00 - 0.774	0.8870
101	0.774 - 0.599	0.6865
102	0.599 - 0.464	0.5315
103	0.464 - 0.359	0.4115
104	0.359 - 0.278	0.3185
105	0.278 - 0.215	0.2465
106	0.215 - 0.167	0.1910
107	0.167 - 0.129	0.1480
108	0.129 - 0.100	0.1145
109	0.100 - 0.0774	0.0887
110	77.4 - 59.9 eV	68.65 eV
111	59.9 - 46.4	53.15
112	46.4 - 35.9	41.15
113	35.9 - 27.8	31.85
114	27.8 - 21.5	24.65
115	21.5 - 16.7	19.10
116	16.7 - 12.9	14.80
117	12.9 - 10.0	11.45
118	10.0 - 7.74	8.870
119	7.74 - 5.99	6.865
120	5.99 - 4.64	5.315
121	4.64 - 3.59	4.115
122	3.59 - 2.78	3.185
123	2.78 - 2.15	2.465
124	2.15 - 1.67	1.910
125	1.67 - 1.29	1.480
126	1.29 - 1.00	1.145
127	1.00 - 0.774	0.8870
128	0.774 - 0.599	0.6865
129	0.599 - 0.464	0.5315
130	0.464 - 0.359	0.4115
131	0.359 - 0.278	0.3185
132	0.278 - 0.215	0.2465
133	0.215 - 0.167	0.1910
134	0.167 - 0.129	0.1480
135	0.129 - 0.010	0.0695

Table A.3 21-Group Gamma-Ray Energy Group Structure

Group	Energy Limits (MeV)	Mid-Point Energy (MeV)
1	14.0 - 12.0	13.0
2	12.0 - 10.0	11.0
3	10.0 - 8.0	9.0
4	8.0 - 7.5	7.75
5	7.5 - 7.0	7.25
6	7.0 - 6.5	6.75
7	6.5 - 6.0	6.25
8	6.0 - 5.5	5.75
9	5.5 - 5.0	5.25
10	5.0 - 4.5	4.75
11	4.5 - 4.0	4.25
12	4.0 - 3.5	3.75
13	3.5 - 3.0	3.25
14	3.0 - 2.5	2.75
15	2.5 - 2.0	2.25
16	2.0 - 1.5	1.75
17	1.5 - 1.0	1.25
18	1.0 - 0.4	0.7
19	0.4 - 0.2	0.3
20	0.2 - 0.1	0.15
21	0.1 - 0.01	0.055

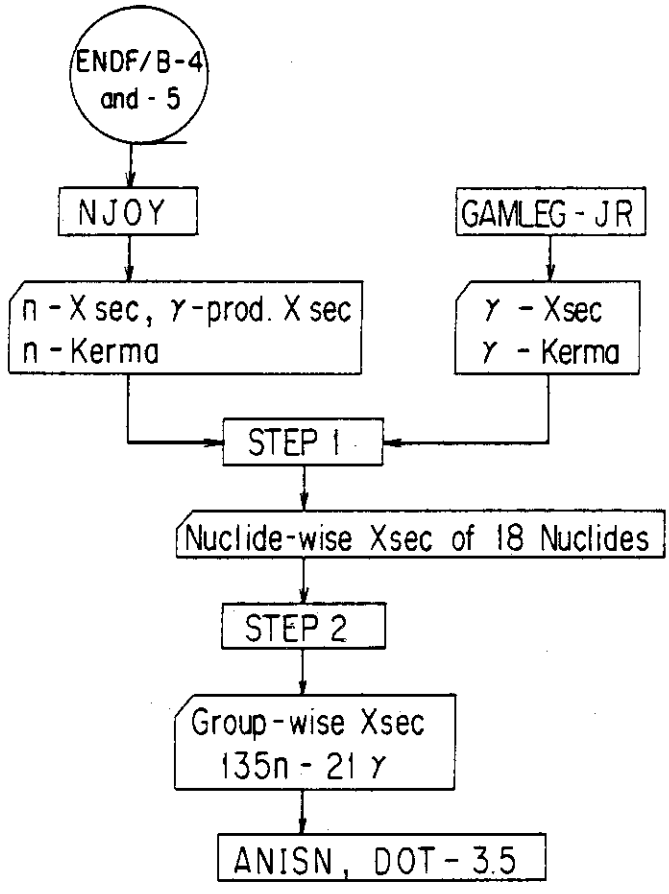

Fig.A.1 Calculational Procedure for Obtaining the Neutron and Gamma-Ray Coupled Cross Section Set

APPENDIX 2. COMPARISON OF FISSION RATES IN LI_2O-C ASSEMBLY CALCULATED WITH VARIOUS DATA AND METHODS

In this APPENDIX, the calculated fission rates using various data and methods are compared for the Li_2O-C assembly represented by the old incorrect nuclide density table in Ref.(4). The old nuclide densities are listed in Table A.4. The major difference of the newly evaluated values in Table 2 from the old ones is that the density of graphite (C) became about 5.5% smaller.

The fission rates are calculated using the same calculational model as shown in Fig.2. The six calculational procedures with various data and methods used in the calculation of the fission rates are listed in Table A.5. The calculated fission rates are compared in the form of the C/E values, the ratio of calculated and experimental values in Figs.A.2a to A.2d. The six calculational procedures are briefly described with the symbols to denote C/E values in Figs.A.2a to A.2d.

1. x———x A 100-group neutron cross section set called GICXLI20 is used. The GICXLI20 set is processed from the nuclear data in ENDF/B-4[7] using the NJOY code.[10] The cross sections for the infinite dilution at 300°K are obtained. The 1/E weighting is used to derive group cross sections from the point data. One dimensional discrete ordinates transport code ANISN[13] is used with the P_5-S_{64} approximation to calculate the neutron flux.

2. x------x The ^{12}C cross section in the GICXLI20 set is replaced by the C cross section processed from the C nuclear data in ENDF/B-5[8] by the NJOY code. All other calculational procedure is the same as 1.

3. x—•—•— x In addition to the C cross section replacement, the $^{7}Li(n,n'\alpha)t$ reaction in the ENDF/B-4 data is replaced by the newly evaluated one.[9] All other calculational procedure is the same as 1.

4. o———o The PALLAS-TS code[17] which solves neutron transport equation by direct numerical integration method is used to obtain the neutron flux. A 120-group cross sections[17] prepared for the PALLAS-TS are used.

These cross sections are processed from the ENDF/B-4[7] by a revised version of the PROF-GROUCH-GII code.[18] The cross sections are for infinite dilution and at 300°K. Constant flux weighting is used to derive group cross sections. The thermal cross section for the 121-th group is obtained by the SRAC code system.[12]

5. Δ------Δ A 42-group neutron cross sections in the GICX40 set[19] for fusion reactor calculation is used in the ANISN(P_5-S_{64}) calculation. The cross sections are processed from the ENDF/B-3 data[7] by the SPTG4Z code[18] using 1/E as the weighting function.

6. □------□ A 42-group neutron cross sections in the GICX40V4 set[19] is used in the ANISN(P_5-S_{64}) calculation. The cross sections are processed from ENDF/B-4 data[7] by the NJOY code.[10] The neutron spectrum in the lithium region of the Li-C assembly[3] is used as the weighting function.

Calculated results in Figs.A.2a to A.2d will be discussed briefly.

Fig.A.2a The C/E of ^{232}Th fission rate

- The calculated results of six calculational procedures agree within 10%.
- The C/E's decrease with the radius R in the graphite region and become smaller than 1.0.
- The C/E for the GICX40 set in which nonelastic neutrons are assumed isotropic deviates most from 1.0.
- The use of C data in ENDF/B-5 and recent ^{7}Li(n,n'α)t reaction cross section improves the agreement by 1 ~ 4%.

Fig.A.2b The C/E of ^{238}U fission rate

- Calculated fission rates agree with the measured one for all locations except at the outermost three locations.
- The C/E for the GICX40 set deviates most from 1.0 due to not taking account of nonelastic neutron anisotropy.
- The use of C data in ENDF/B-5 and recent ^{7}Li(n,n'α)t cross section data improves the agreement by up to 6%.

Fig.A.2c The C/E of ^{237}Np fission rate

- Calculation agree with the measurement except at R = 10.1 cm and at the outermost locations.
- Relatively large disagreement for the GICX40 case and the improvement in the agreement by the replacement with recent nuclear data are seen.

Fig.A.2d The C/E of ^{235}U fission rate

- Although good agreement is seen in the Li_2O region, large deviation from 1.0 seen in the graphite region.
- The use of C cross section of ENDF/B-5 improves the agreement by about 5% in the graphite region. The use of the recent $^{7}Li(n,n'\alpha)t$ evaluation further improves the agreement by another 4%.
- The C/E for the GICX40V4 case shows a trend completely different from the other C/E's. The reason for the difference is in the use of the spectrum of the lithium region as the weighting function whereas the 1/E weighting is used in all other cases. This will be further discussed with the aid of Fig.A.2e.

Figure A.2e shows the comparison the C/E of the GICX40V4 set with the C/E's calculated with the GICX50 set. The GICX50 set is obtained by the same procedure as the GICX40V4 set except for the weighting function used. The figure shows that the difference of the weighting function is the cause of the difference in the trend of the C/E. This figure also shows that the choice of the thermal group ^{235}U fission cross section also influence the magnitude of calculated ^{235}U fission rate in the graphite region. The 42-th energy group extends from 0.001-0.215 eV. The 1/E weighted value for the 42-th group value of ^{235}U fission cross section is 1060 barns and the thermal ^{235}U fission cross section obtained by the SRAC code system is 415 barns.

Major conclusions obtained from the comparison described in this APPENDIX are as follows:

(1) The difference in the calculated fission rates caused by the difference in the neutron transport codes, namely PALLAS-TS employing the direct integration method and the ANISN using the discrete ordinates method is 16% at most.

(2) The use of C cross section data of ENDF/B-5 in place of ^{12}C data

in ENDF/B-4 improves the agreement for all four fission rates by 5% at most. The use of the recent evaluation of ^{7}Li cross sections[9] improves the agreement by another 4%.

(3) The neglect of nonelastic neutron anisotropy in the GICX40 set resulted in about 5% larger discrepancy of calculated fission rates of ^{232}Th, ^{238}U and ^{237}Np in the graphite region.

(4) Comparison of the 100-group calculation results in Fig.6a-6d with the 100-group results in Figs.A.2a-A.2d obtained with recent C and ^{7}Li cross sections shows the effect of the nuclide density change. The nuclide density change improves the agreement by about 5% in the ^{232}Th fission rate and by more than 15% in the ^{235}U fission rate.

Table A.4 Nuclide Densities of each Region in Li_2O-C Assembly (Old values)

Nuclide	Nuclide density (10^{24} atoms/cm^3)			
	Void	Li_2O	Graphite	Lattice
^{6}Li		3.3547×10^{-3}		
^{7}Li		4.1857×10^{-2}		
O		2.2606×10^{-2}		
C			7.3445×10^{-2}	
Cr	1.827×10^{-3}	2.011×10^{-3}	1.827×10^{-3}	1.224×10^{-3}
Ni	7.964×10^{-4}	8.781×10^{-4}	7.964×10^{-4}	5.336×10^{-4}
Fe	6.652×10^{-3}	7.346×10^{-3}	6.652×10^{-3}	4.457×10^{-3}

Table A.5 Description of six calculational procedures

Items	Calculational procedures					
	1	2	3	4	5	6
Nuclear data file	ENDF/B-4	ENDF/B-4*1	ENDF/B-4*2	ENDF/B-4	ENDF/B-3	ENDF/B-4
Name of Xsec set	GICXLI20	GICXLI20	GICXLI20	——— (17)	GICX40 (19)	GICX40V4 (19)
Process code	NJOY (10)	NJOY	NJOY	PROF-GROUCH-GII (18)	SPTG4Z (18)	NJOY
Energy group No.	100	100	100	121	42	42
Weighting function	1/E	1/E	1/E	Constant	1/E	Li-spectr.*3
Transport code	ANISN (13)	ANISN	ANISN	PALLAS-TS (17)	ANISN	ANISN
Approximation	$P_5 - S_{64}$	$P_5 - S_{64}$	$P_5 - S_{64}$	$P_\infty - S_{20}$	$P_5 - S_{64}$	$P_5 - S_{64}$
Symbol used in Figs.	x——x	x----x	x—•—x	○———○	△-----△	□-----□

*1 ENDF/B-5 data used for ^{12}C

*2 ENDF/B-5 data used for ^{12}C, $^{7}Li(n,n'\alpha)t$ reaction cross section (9)

*3 Calculated neutron spectrum in Li-region of Li-C Assembly (3)

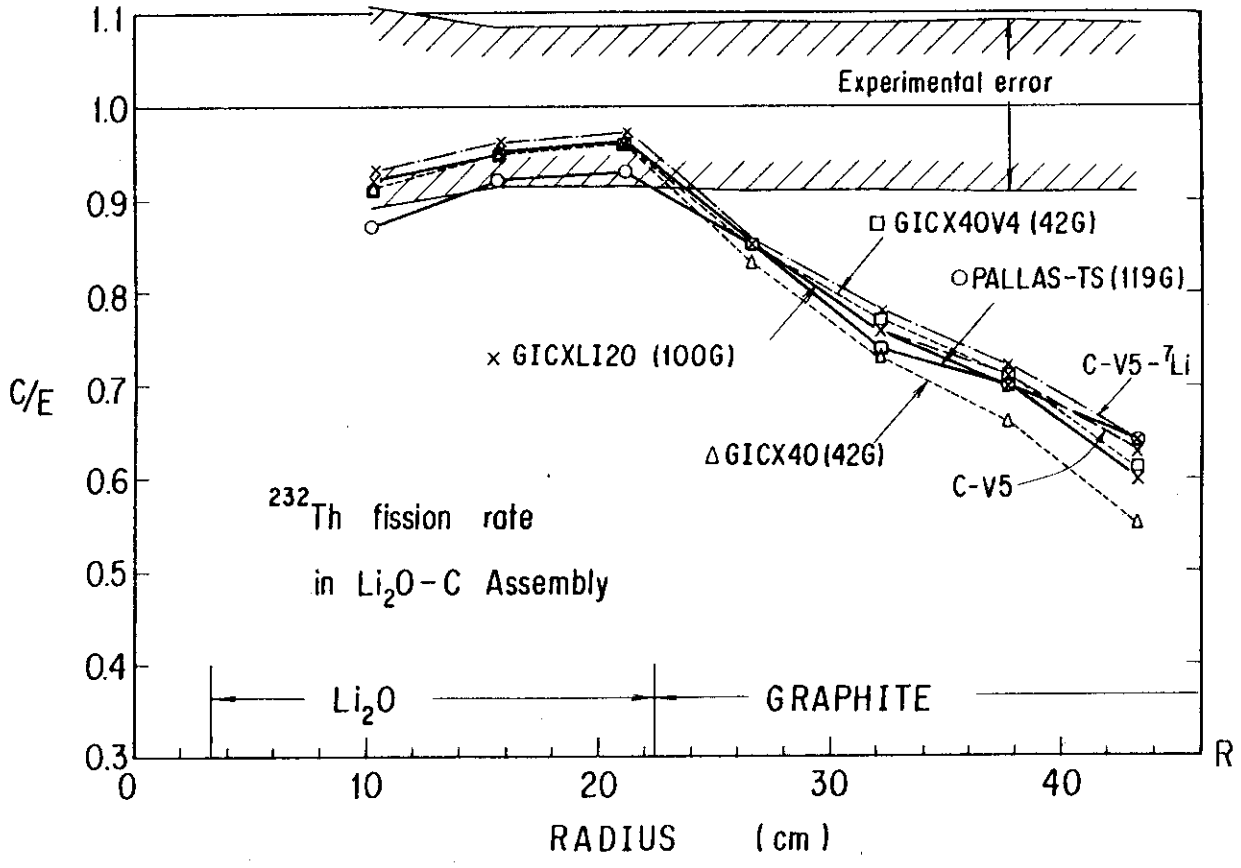

Fig.A.2a The C/E values of ^{232}Th Fission Rates in Li_2O-C Assembly (Using Old Nuclide Densities)

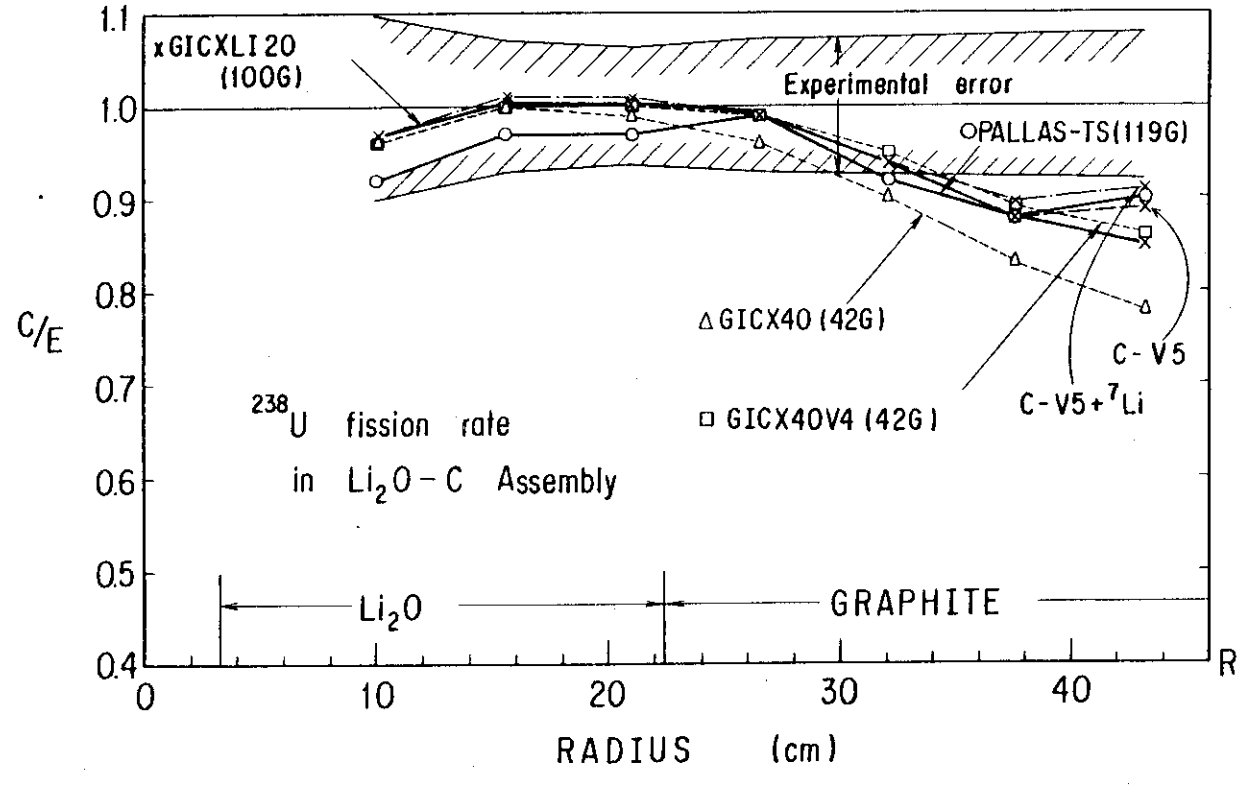

Fig.A.2b The C/E values of ^{238}U Fission Rates in Li_2O-C Assembly (Using Old Nuclide Densities)

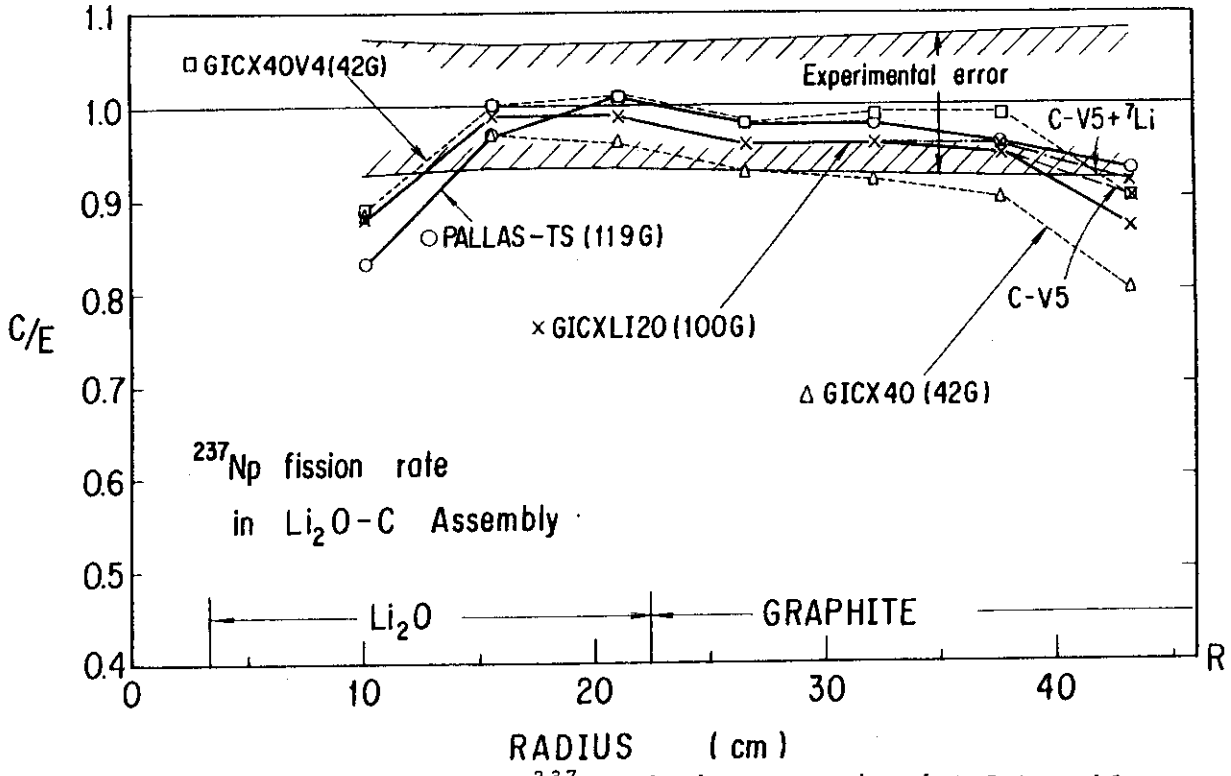

Fig.A.2c The C/E values of ^{237}Np Fission Rates in Li_2O-C Assembly (Using Old Nuclide Densities)

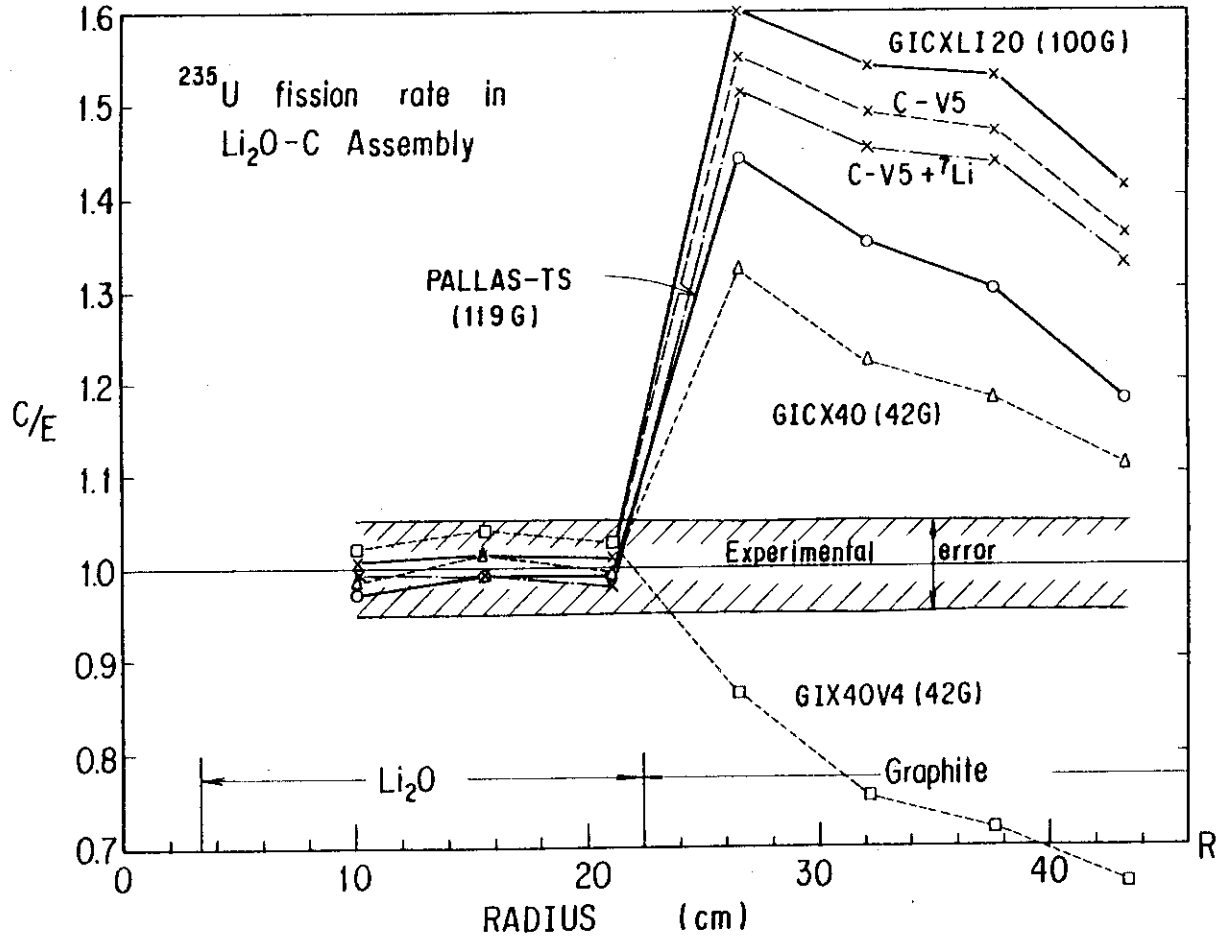

Fig.A.2d The C/E values of ^{235}U Fission Rates in Li_2O-C Assembly (Using Old Nuclide Densities)

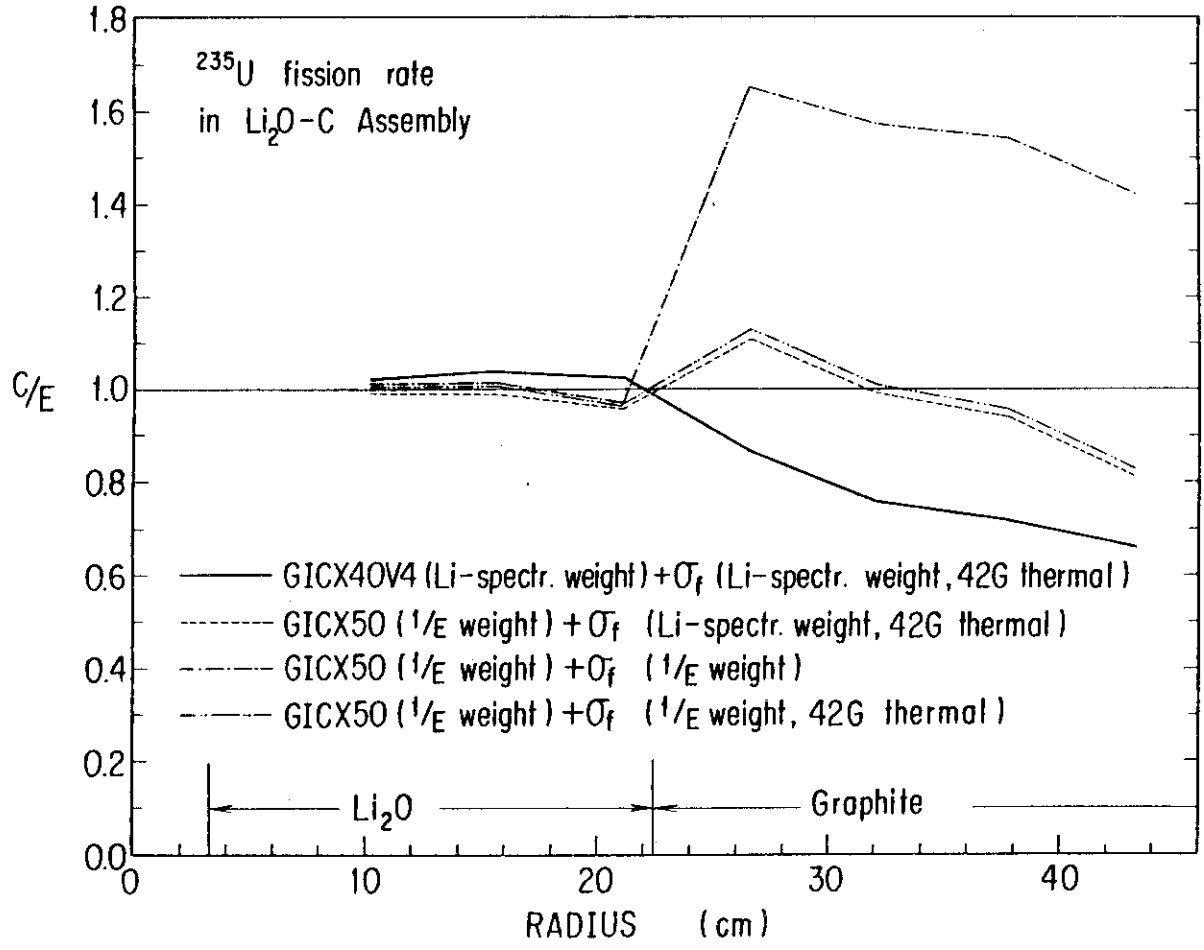

Fig.A.2e The C/E values of ^{235}U Fission Rates in Li_2O-C Assembly for Calculations Using Different 42-Group Cross Sections